# A parametric study of part distortions in fused deposition modelling using three-dimensional finite element analysis

**Y Zhang** and **K Chou***
Mechanical Engineering Department, University of Alabama, Tuscaloosa, Alabama, USA

*The manuscript was received on 24 August 2007 and was accepted after revision for publication on 24 April 2008.*

DOI: 10.1243/09544054JEM990

**Abstract:** A finite element analysis (FEA) model was previously developed by the current authors to simulate the fused deposition modelling (FDM) process. The model considered coupled thermal and mechanical phenomena and incorporated an element activation function to mimic the additive nature of FDM. Due to repetitive heating and cooling in the FDM process, residual stresses accumulate in a part during deposition. In this study, an FEA model is used to evaluate the distortions of a part. A parametric study, with three factors and three levels, is performed to evaluate the effects of the deposition parameters on residual stresses and part distortions. Prototype models with larger sizes are fabricated, measured, and compared with the simulations.

The simulation results are summarized as follows. First, the scan speed is the most significant factor affecting part distortions, followed by the layer thickness. Second, the road width alone is insignificant. However, the interaction between the road width and the layer thickness is significant as well. Third, there are other two-way and three-way interactions that are of secondary significance. In general, residual stresses in FDM parts increase with the layer thickness. Residual stresses also increase with the road width, but to a lesser extent, although largely affected by the layer thickness. The FDM part distortions from the experiment show a similar trend as concluded in the simulations, but without quantitative correlation.

**Keywords:** fused deposition modelling, numerical simulation, parametric study, part distortion

## 1 INTRODUCTION

Fused deposition modelling (FDM) is one of the most widely used solid freeform fabrication (SFF) systems because it uses inexpensive machinery and durable part materials. In FDM, a thermoplastic material is heated to a semi-molten state, extruded as an ultra-thin filament, and deposited to build a part. The extrusion nozzle move according to a toolpath defined by the part cross-sectional boundary and material is deposited on top of the existing layer. Heat is dissipated by conduction and forced convection and the reduction in temperature caused by these processes causes the material to quickly solidify onto the surrounding filaments. Bonding between the filaments is caused by local re-melting of previously solidified material and diffusion [**1**]. The role of the part geometry in SFF is a frequently studied subject. Recently, Mahesh *et al.* [**2**] used a benchmark part to evaluate several SFF processes and measured tolerances such as flatness and symmetry were compared. The authors noted that the residual-stress-induced-distortions (e.g. warpage and delamination) are prominent. As in other SFF processes, in FDM, the heating and rapid cooling cycles of the materials result in non-uniform thermal gradients which cause a stress build-up that leads to distortions. Qiu and Langrana [**3**] studied the toolpath effects in FDM and proposed an algorithm to match the toolpath with the extrusion speed so as to eliminate voids and to correct overfill and underfill defects. Pennington *et al.* [**4**] conducted an experimental study to investigate factors that influence

*Corresponding author: The University of Alabama, Mechanical Engineering Department, 290 Hardaway Hall, Tuscaloosa, Alabama, USA. Email: kchou@eng.ua.edu*

dimensional accuracy in FDM. The authors reported that the part size, location, and envelope temperature have a significant effect. Jiang and Gu [**5**] studied extrusion phenomena in FDM and reported that the process parameters are critical to the part accuracy.

Most SFF processes involve localized energy transport, mass transfer, phase changes, and thermally-induced mechanical loading. Due to high process temperatures, repetitive thermal cycles, and continuous geometric changes, the process modelling and simulation of SFF are difficult topics. Numerical approaches have been applied to model residual stresses in SFF processes. Dalgarno *et al.* [**6**] conducted structural analyses to model the development of the curling of parts in a selective laser sintering process. It was reported that applying double sintering to the first two layers of a part to relieve the strains may significantly reduce the curling level. Sonmez and Hahn [**7**] developed a thermomechanical model for the laminated object manufacturing process, correlating process parameters with temperatures and stress distributions in the laminate during fabrications, and further suggested that a large roller diameter and a slower roller speed would be favourable for laminate bonding. Chin *et al.* [**8**] extended an earlier one-dimensional model to establish thermomechanical models for individual layers, droplet columns, and adjacent droplets in the shape deposition manufacturing (SDM) process. The authors reported that while localized substrate preheating was ineffective, process-induced preheating seemed to be effective in reducing thermal gradients and residual stresses. Nickel *et al.* [**9**] developed a three-dimensional finite element analysis (FEA) model to study the effect of deposition patterns on the resulting stresses and deflections in SDM. It was suggested that a raster pattern, with the primary laser moving direction normal to the part major axis, would produce the least deflections.

There are some reports in the literature on FEA studies of part distortions in liquid-based SFF processes. Wiedemann *et al.* [**10**] developed methods to evaluate photopolymers with respect to the dynamics of polymerization and shrinkage. The sensitivity of polymerization to the process conditions was also studied. A numerical simulation of part distortions was applied to reveal the interaction between the material properties and the process parameters. The time-dependent shrinkage and increase in strength during the polymerization were investigated. It was concluded that the deposition process must be optimized to reduce internal stresses using a stereolithographic apparatus (SLA). Bugeda *et al.* [**11**] modelled the mechanical aspect of using SLA to study the influence of different constructive and numerical parameters in the curl distortion caused by resin shrinkage. The curl distortion was found to increase with the volumetric shrinkage, but was found to decrease when the layer thickness increased. Xu *et al.* [**12**] incorporated thermal stresses for shrinkages due to resin phase changes into a FEA to simulate the part deformations in SLA. Huang and Lan [**13**] used a dynamic finite element code to simulate the photopolymerization process in order to efficiently select process parameters and to obtain distortion data.

A three-dimensional FEA model was developed by Zhang and Chou [**14**] in order to simulate the FDM deposition process by controlling element activations for the involved mechanical and thermal processes. The model could be used to predict residual stresses and evaluate part distortions in FDM. This model is now applied to investigate, by incorporating the design-of-experiments approach, the effects of process parameters on the residual stresses and distortion of parts in FDM.

## 2 NUMERICAL SIMULATIONS

### 2.1 Finite element model

The commercial software, ANSYS, was utilized to develop the simulation codes. The simulations were conducted in a stepwise thermo-mechanical manner. The element geometry chosen, a rectangular parallelepiped, had dual attributes (solid 45/solid 70), compatible with the thermal and mechanical analyses. The governing equation of the thermal analysis was a three-dimensional transient heat conduction representation with heat generation from the phase changes [**14**]. The bottom surface of the model which was in contact with the platform was set to be at a constant chamber temperature (75 °C). The boundary conditions of the other outer surfaces were obtained by forced convection with an ambient temperature of 75 °C and a heat convection coefficient of 86 $W/m^2 K$ see the appendix for further details. The properties of ABS plastic were used in the simulations. The initial temperature of a newly activated element was set at the extrusion head temperature (280 °C) and for other activated elements, the initial temperatures were those obtained in the previous step of the thermal analysis. The mechanical analysis used a static structural analysis (elastic stress equilibrium) approach with induced thermal strains. For the mechanical boundary conditions, the bottom surface of the part was fully constrained. For newly activated elements, the initial displacement was zero. For other elements, the result of the previous mechanical analysis step was used as the initial condition. The 'element birth/death' function was used to mimic the additive feature in FDM, i.e. continuous filament depositions. The model geometry was first specified, meshed, and the elements were activated according

to the filament deposition sequence. For each element activated, a transient thermal analysis started with the current temperature distributions as the initial condition. The calculation continued until the next element was extruded, which is a function of the element size and the linear deposition speed. The obtained temperature distribution was then used in the next-step mechanical analysis that calculated the displacement at each node of all activated elements. The next element following the designated path was then activated and the convection surface was updated for the next temperature analysis, and these cycles were repeated until all the elements were activated. Displacements, strains, and stresses in the constrained part were analysed. Then a thermal analysis was executed to change the ambient temperature from the chamber to the laboratory. The displacement constraint of the model was also released in the final mechanical analysis to simulate removing the part from the platform.

### 2.2 Parametric study

The effects of the major process parameters in FDM such as the road width, the layer thickness, and the scanning speed were investigated using the developed FEA model. Three levels (low, medium, and high) of each factor were used: 0.25, 0.5, and 1.0 mm for the road width, 0.127, 0.254, and 0.508 mm for the layer thickness, and 32, 64, and 96 mm/s for the scan speed. The scanning speed alters the heating and cooling frequency during depositions and results in different degrees of thermal gradients in the part, which in turn affect the residual stresses. The layer thickness and the road width affect the number of layers and the tool paths required at each layer. A thick layer means fewer layers, which may reduce the number of heating and cooling cycles. On the other hand, a smaller road width will input less heat into the system within a specific amount of time, but requires more loops to fill a certain area. This will complicate the temperature and stress evolutions and influence the residual stress distributions. Moreover, the effects due to the interactions between the selected parameters are not clearly known.

To systematically investigate the FDM process parameter effects, a second-order approach, a central composite design (CCD), was applied in the design of experiments [**15**]. A typical CCD is made up of three portions: the factorial, the central point, and the axial portions. The factorial portion is a three-factor, two-level, one-half fractional factorial design. Together with one centre run and six axial runs, CCD requires only 15 runs instead of 27 in a three-factor, three-level full factorial design. Moreover, the CCD method is able to reveal high-order interactions. In this study, the six axial runs included either a high or low level of each factor. Due to the significant computation times required for large models, a small representative $40 \times 10 \times 1.016$ plate, corresponding to the longitudinal, transverse, and height dimensions, was used in the simulations. To discretize the deposition process, a small element, e.g. $1 \times 0.25 \times 0.127$, was set as a single unit for activations. In addition, the toolpath used was the long-raster pattern, i.e. the primary direction of movement of the extrusion head is along the longitudinal axis of the part.

## 3 RESULTS AND DISCUSSION

### 3.1 Simulation results

Table 1 lists the parameters of each case studied as well as the corresponding simulation result, the maximum first principal stress ($\sigma_1$). Figure 1 presents a few examples of first principal stress distributions at different deposition settings (cases 5, 11, and 4). The shown stress contours are present at the bottom surface of the part where high residual stresses always occur [**14**]. It is noted that the process parameters have significant effects on the residual stresses in the prototypes. Case 5, corresponding to a 1-mm road width, 0.127-mm layer thickness, and 32-mm/s scan speed, results in the lowest residual stresses. Case 11, corresponding to a 1-mm road width, 0.254-mm layer thickness, and 64-mm/s scan speed, results in an intermediate level of residual stresses. On the other hand, case 4, corresponding to a 0.25-mm road width, 0.508-mm layer thickness, and 96-mm/s scan speed, results in the most severe stress accumulations.

All the tested cases were further analysed to investigate the situation when the part distortions imitating that the part is removed from the platform. Figure 2 shows examples of distortion simulation results, cases 4, 5, and 11. It is noted that the greater the residual stresses, the more severe the part distortions. Figure 3 plots the part distortion values (flatness) against the maximum first principal stress from 15 cases. It is observed that in general, the simulated part distortions show a monotonic increasing trend with the maximum first principal stress in the FDM parts. However, there are some cases that show an opposite trend locally, i.e. a low stress with more distortion, therefore there does not appear to be a clear correlation between these factors. It should be noted that, in addition to the first principal stress that is calculated from the six stress states at a location, the FDM part distortions are affected by other factors, e.g. different stress components and stress distributions. Moreover, FDM part distortions show a vaulting shape in both longitudinal and transverse directions, indicating a complex phenomenon

**Table 1** The design-of-experiments matrix and the simulation results, maximum first principal stress

| Case | Factors | | | Results |
|---|---|---|---|---|
| | *A* (road width) | *B* (layer thickness) | *C* (scan speed) | max. $\sigma_1$ (kPa) |
| 1 | −1 | −1 | −1 | $6.54 \times 10^1$ |
| 2 | −1 | −1 | 1 | $2.52 \times 10^3$ |
| 3 | −1 | 1 | −1 | $1.67 \times 10^2$ |
| 4 | −1 | 1 | 1 | $2.04 \times 10^5$ |
| 5 | 1 | −1 | −1 | $5.27 \times 10^1$ |
| 6 | 1 | −1 | 1 | $8.66 \times 10^4$ |
| 7 | 1 | 1 | −1 | $5.29 \times 10^1$ |
| 8 | 1 | 1 | 1 | $6.22 \times 10^4$ |
| 9 | 0 | 0 | 0 | $8.31 \times 10^3$ |
| 10 | −1 | 0 | 0 | $2.59 \times 10^2$ |
| 11 | 1 | 0 | 0 | $4.59 \times 10^3$ |
| 12 | 0 | −1 | 0 | $1.42 \times 10^2$ |
| 13 | 0 | 1 | 0 | $8.33 \times 10^3$ |
| 14 | 0 | 0 | −1 | $7.25 \times 10^1$ |
| 15 | 0 | 0 | 1 | $1.06 \times 10^5$ |

(−1: low, 0: medium, 1: high)

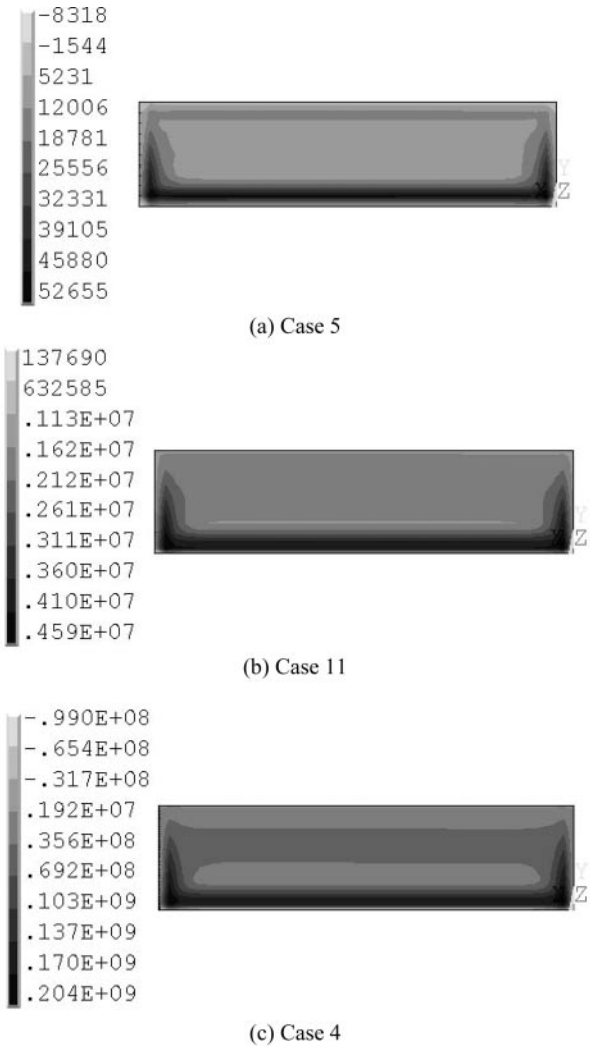


**Fig. 1** First principal stress distribution ($\sigma_1$, Pa) at the bottom surface of a part with different deposition conditions

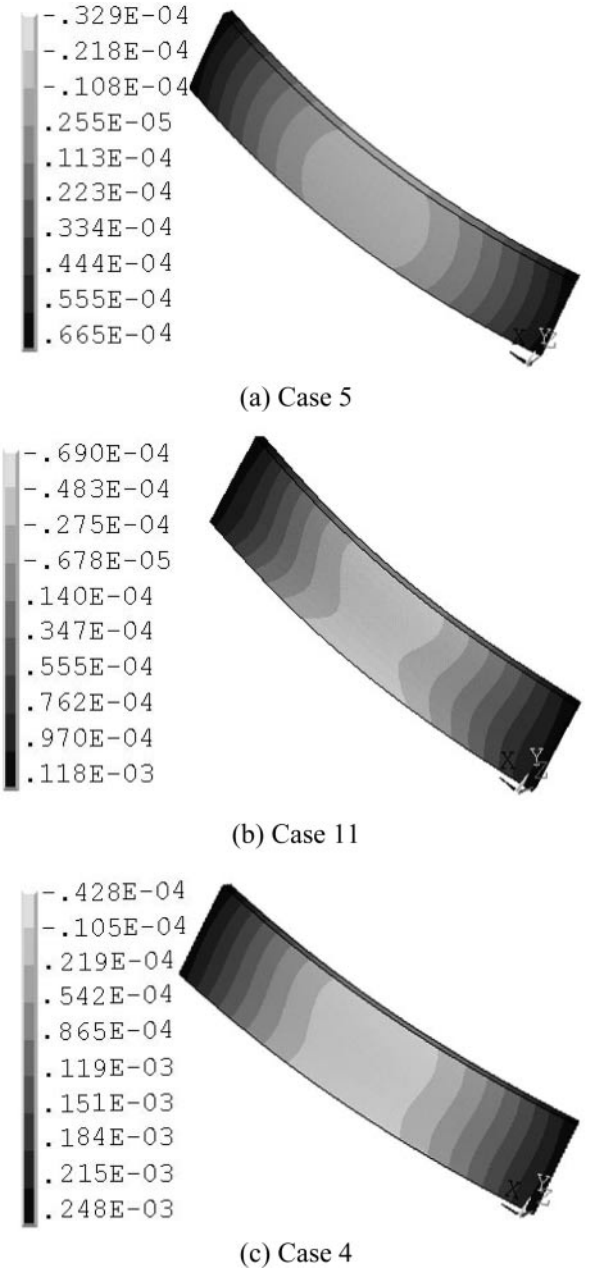


**Fig. 2** Simulated part distortions at different deposition conditions (unit: m)

affected by more than longitudinal and transverse stress components. Therefore, a critical stress component, the first principal stress, was used for the following statistical analysis.

### 3.2 Statistical analysis

The analysis of variance (ANOVA) approach was applied to the maximum first principle stress ($\sigma_1$) of all cases to identify significant factors and interactions between factors. The results, listed in Table 2, show that the scan speed (*C*) is the most significant factor, followed by the layer thickness (*B*). The road width

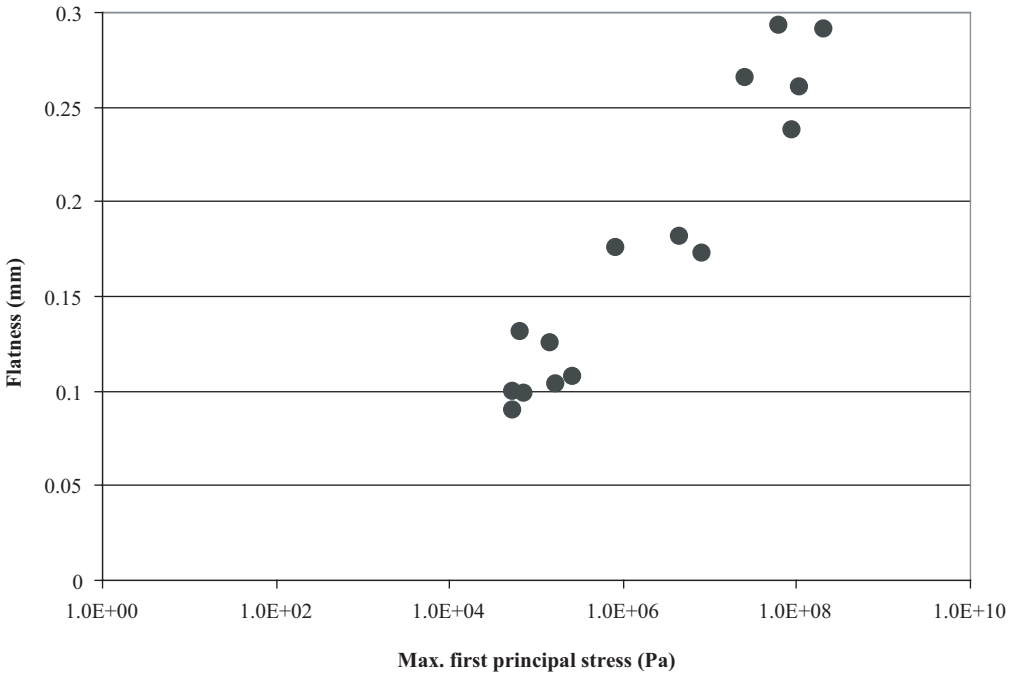


**Fig. 3** Simulated part flatness versus the maximum first principal stress in the part

**Table 2** ANOVA results of maximum first principal stresses (in Pa)

| Factor | *P* value |
|---|---|
| *A* (road width) | 0.2926 |
| *B* (layer thickness) | 0.0138 |
| *C* (scan speed) | 0.0005 |
| *AB* | 0.0046 |
| *AC* | 0.2188 |
| *BC* | 0.0110 |
| *ABC* | 0.0046 |
| *AA* | 0.5779 |
| *BB* | 0.7116 |
| *CC* | 0.0065 |

(*A*) in isolation is insignificant. However, the interaction between the road width (*A*) and the layer thickness (*B*) is considered to be significant. In addition, there are other high-order interactions, i.e. *BC*, *CC*, and *ABC* that are of secondary significance.

After excluding the insignificant interactions, the ANOVA process was again performed using logarithmic values, to obtain a prediction equation for the maximum $\sigma_1$ (in Pascals). The regression gives a residue *R* of 0.94

$$\log(\max\sigma_1) = 6.21 + 0.0676A + 0.494B + 1.31C - 0.432AB + 0.0445BC - 0.0808ABC + 0.168C^2 \quad (1)$$

To validate the regression model, three additional cases of different parameters, i.e. varied (*A*, *B*, *C*) sets, were studied using the three-dimensional FEA model. The three cases chosen correspond to some of the test conditions in the experimental investigation reported in the following section. The simulations were compared with the results predicted using equation (1). The results are summarized in Table 3. The average relative error is less than 10 per cent with the maximum value being 12.6 per cent.

### 3.3 Experimental comparisons

To examine the FEA model, several prototypes were fabricated in an FDM machine and then measured to allow comparisons to be made. Owing to accuracy limitations in the measurement of small parts, parts with larger dimensions, but with the same length: width ratio, were used: 100 × 25 mm blocks with a height of 30 mm. In addition to the nominal operation condition (a 0.50-mm road width and a 0.25-mm layer thickness), two road widths (0.36 and 0.76 mm), and two layer thicknesses (0.18 and 0.33 mm) were varied to investigate the parameter effects. The fabricated prototypes were removed from the platform and mounted on a metal flat using sealants. The bottom surface of a part (in reference to the deposition) was probed using a coordinate measuring machine in automatic measuring mode using a total of 50 equally spaced points. The raw data were processed in Matlab and two- and three-dimensional plots of the part surface were produced. The distortion values (flatness) at different parameter settings were compared.

Figure 4 is a typical example of the shape of a bottom surface of a part. All the measured FDM parts showed the same distortion pattern (vaulting shape). However, the flatness value (about 0.63 mm in this example) is

**Table 3** Validation result of stress regression equation

| Factor and level | | | Log (max, $\sigma_1$) | | |
|---|---|---|---|---|---|
| Road width (mm), [*A*] | Layer thickness (mm), [*B*] | Scan speed (mm/s), [*C*] | FEA simulation | Regression equation | Relative error (%) |
| 0.36, [−0.55] | 0.18, [−0.6] | 32, [−1] | 5.318 | 4.648 | 12.6 |
| 0.76, [0.53] | 0.18, [−0.6] | 32, [−1] | 4.589 | 4.947 | 7.8 |
| 0.36, [−0.55] | 0.33, [0.3] | 32, [−1] | 4.816 | 5.225 | 8.5 |

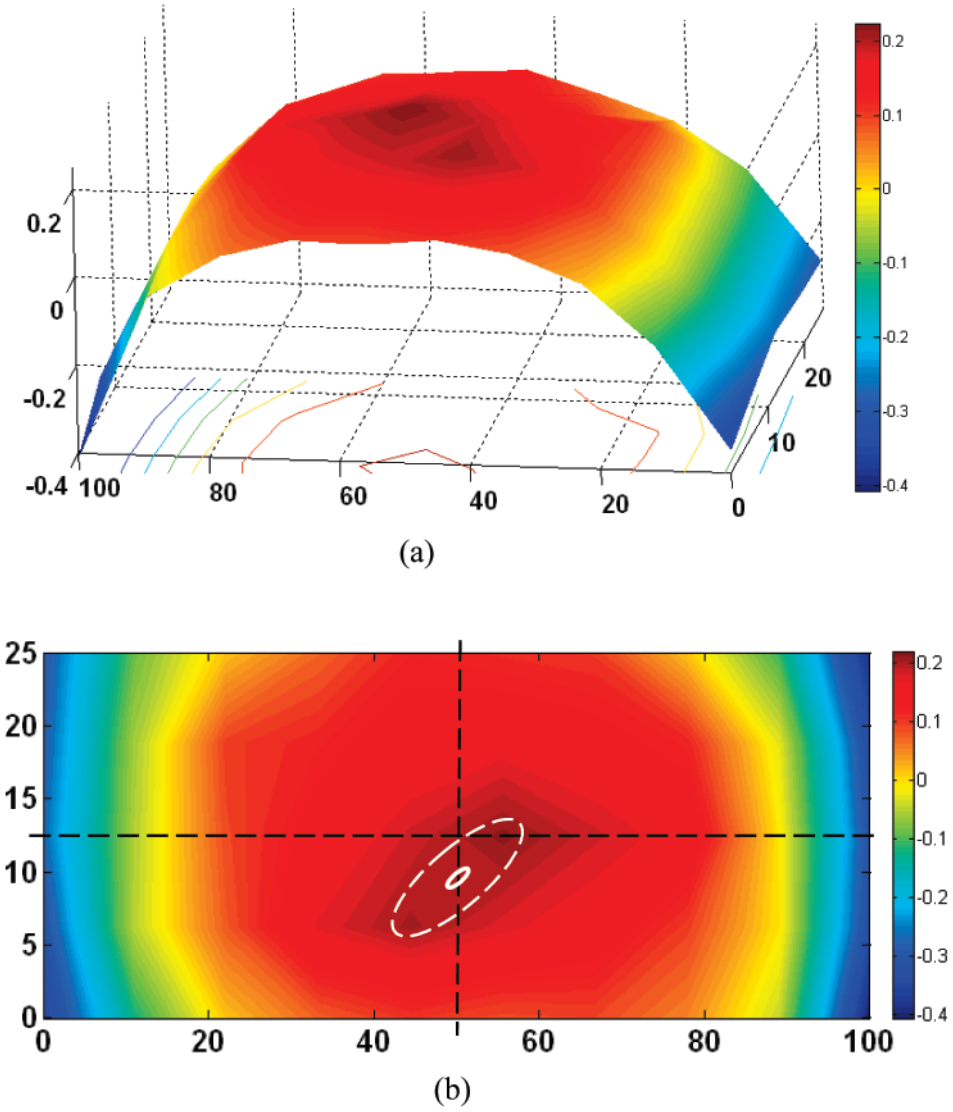


**Fig. 4** An example of the distortion of a bottom surface of a part: (a) three-dimensional height profile showing the vaulting shape (unit: mm); and (b) two-dimensional contour showing shifting of the distortion centre (mm)

not necessarily comparable to the simulation results for small parts. It is noted that the distortion core (the small white-line oval in Fig. 4(b)) shifts away from the geometric centre of the part along the longitudinal axis. The shift of the distortion centre is consistent with simulated behaviour (Fig. 2) and it is due to the asymmetric stress distribution created by the tool path pattern used in the deposition (long-raster in this case). Figure 5 shows the out-of-plane distortion, around the part centre, in the longitudinal and transverse directions. As observed in Fig. 4, the asymmetric distortion occurs in the transverse direction.

The measured distortion results for different parameters are compared in Fig. 6 together with the

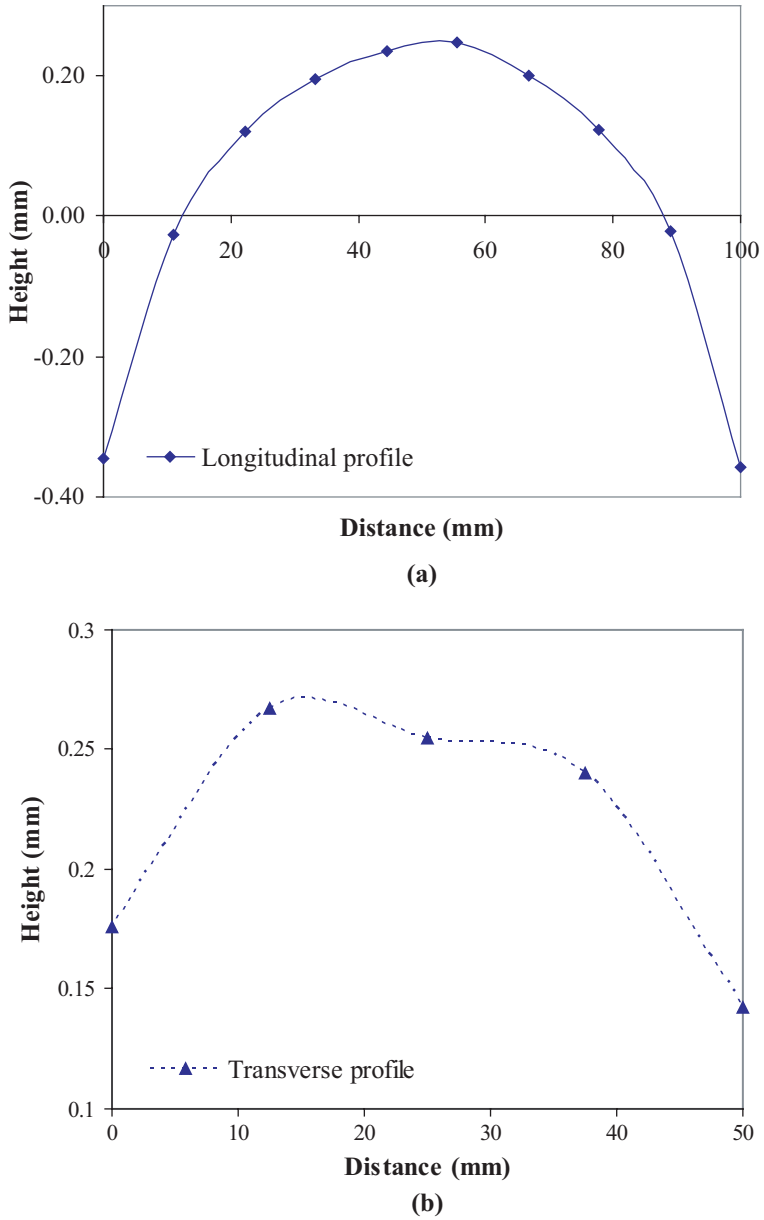


**Fig. 5** Out-of-plane distortion in the: (a) longitudinal; and (b) transverse directions

simulated maximum residual stresses predicted using equation (1). It is noted that the distortions increase with both the layer thickness and the road width, which is consistent with simulation results. However, interactions between the layer thickness and the road width are not significantly discernible. Note that the simulations indicate that the stress accumulations increase with the layer thickness, and increase with the road width, but to a lesser extent. At small layer thicknesses, increasing the road width will increase the level of stress accumulations. However, at larger layer thicknesses, the road width has little effect on the residual stresses of the part. In this study, the FEA simulations were only performed on small parts due to computation time constraints. On the other hand, the experimental investigation used thick parts and was only limited by measurement accuracy. Thus, the simulations and experimental results can only be qualitatively compared, which can clearly be demonstrated from the combined graph showing that distortions increase with the stress level.

## 4 CONCLUSIONS

In this study, the FDM process was simulated using a three-dimensional FEA modelling approach that incorporates the additive feature and thermomechanical phenomena during the material depositions. The model was tested to evaluate the part distortions, showing a vaulting shape and distortion-core shifting caused by asymmetric stress distributions. The

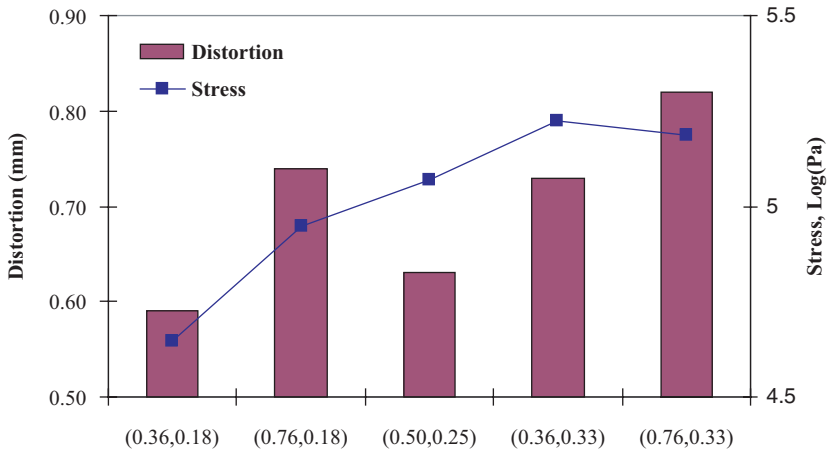


**Fig. 6** Part distortion results from the experiment compared with the stress simulations (variable pair in abscissa is road width and layer thickness, both in mm)

model was used to study the effects of process parameters on the part distortions in FDM. The design of experiments, using the central composite design scheme, consisted of three factors and three levels. ANOVA was then used to identify significant factors and/or factor interactions, and to establish a regression model of the residual stresses. The simulations and analysis can be summarized as follows.

1. The simulation results show that part distortions are related to the stress accumulation during the deposition.
2. Among the three tested parameters, the scan speed is the most significant factor to the residual stresses followed by the layer thickness.
3. The road width alone does not affect the residual stress and part distortions in a statistically significant manner. However, the interaction between the road width and the layer thickness seems to be as significant as the layer thickness to part distortions.
4. There are other two-way and three-way interactions that are of secondary significance.
5. The simulations indicate that the stress accumulations increase with increasing layer thickness and increasing road width (although to a lesser extent for the latter factor). The distortion results from the experiment show a similar trend; distortions increase with both the road width and the layer thickness, however, the effects between these two factors are not discernible. A quantitative correlation is yet to be established.

## REFERENCES


1 **Sun, Q., Rizvi, G. M., Giuliani, V., Bellehumeur, C. T.,** and **Gu, P.** Experimental study and modeling of bond formation between ABS filaments in the FDM Process. In Proceedings of the *Annual technical conference – ANTEC,* 2004, vol. 1, pp. 1158–1162.

2 **Mahesh, M., Wong, Y. S., Fuh, Y. H.,** and **Loh, H. T.** Benchmarking for comparative evaluation of RP systems and processes. *Rapid Prototyping J.*, 2004, **10**(2), 123–35.

3 **Qiu, D.** and **Langrana, N. A.** Void eliminating tollpath for extrusion-based multi-material layered manufacturing. *Rapid Prototyping J.*, 2002, **8**(1), 38–45.

4 **Pennington, R. C., Hoekstra, N. L.,** and **Newcomer, J. L.** Significant factors on the dimensional accuracy of fused deposition modeling. Proceedings of the *Annual technical conference – ANTEC* 2003, vol. 1, pp. 880–883.

5 **Jiang, K. Y.** and **Gu, Y. H.** Controlling parameters for polymer melting and extrusion in FDM. *Key Engng. Mater.*, 2004, **258–259**, 667–671.

6 **Dalgarno, K. W., Childs, T. H. C., Rowntree, I.,** and **Rothwell, L.** Finite element analysis of curl development in the selective laser sintering process. In Proceedings of *Solid freeform fabrication symposium,* University of Texas, Austin, TX, 1996, pp. 559–566.

7 **Sonmez, F. O.** and **Hahn, T. H.** Thermomechanical analysis of the laminated object manufacturing (LOM) process. *Rapid Prototyping J.*, 1998, **4**(1), 26–36.

8 **Chin, R. K., Beuth, J. L.,** and **Amon, C. H.** Successive deposition of metals in solid freeform fabrication processes, part 2: thermomechanical models of adjacent droplets. *J. Manuf. Sci. Engng*, 2001, **123**, 632–638.

9 **Nickel, A. H., Barnett, D. M.,** and **Prinz, F. B.** Thermal stresses and deposition patterns in layered manufacturing. *Mater. Sci. Engng. A*, 2001, **317**, 59–64.

10 **Wiedmann, B., Dusel, K. H.,** and **Eschl, J.** Investigation into material and process on part distortion. *Rapid Prototyping J.*, 1995, **1**(3), 17–22.

11 **Bugeda, G., Cervera, M., Lombera, G.,** and **Onate, E.** Numerical analysis of stereolithography processes using the finite element method. *Rapid Prototyping J.*, 1995, **1**(2), 13–23.

12 **Xu, H., Zhang, Y., Lu, B.,** and **Chen, D.** Numerical simulation of solidified deformation of resin parts in stereolithography rapid prototyping. *Chin. J. Mech. Engng*, 2004, **40**(6), 107–112.

13 **Huang, Y.-M.** and **Lan, H.-Y.** Dynamic reverse compensation to increase the accuracy of the rapid prototyping system. *J. Mater. Process. Technol.*, 2005, **167**(2–3), 167–176.
14 **Zhang, Y.** and **Chou, Y. K.** 3D FEA simulations of fused deposition modeling process. In Proceedings of ASME International Conference on *Manufacturing science and engineering*, Ypsilanti, MI, 2006, MSEC2006-21132.
15 **Schmidt, S. R.** and **Launsby, R. G.** *Understanding industrial designed experiments*, 1997 (Air Force Academy Press, Colorado Springs, Colorado).
16 **Incropera, F. P.** and **DeWitt, D. P.** *Introduction to heat transfer*, fourth edition, 1996 (John Wiley, New York).

## APPENDIX

Heat convection coefficient estimate.

The heat flux, from the surfaces of the FDM part to the chamber air, is given by the following equation

$$q = \overline{h}(T_s - T_\infty)$$

where $\bar{h}$ is the average heat convection coefficient, $T_s$ is the surface temperature, and $T_\infty$ is the bulk fluid temperature. For forced convection, the average heat convection coefficient, $\bar{h}$, is correlated by the following equation [**16**]

$$\overline{Nu_L} = \frac{\bar{h}L}{k} = 0.664 Re_L^{1/2} Pr^{1/3}$$

where $\overline{Nu_L}$ is the Nusselt number over the region of interest, $L$ is the length of the workpiece, $k$ is the thermal conductivity of the convection media, $Re_L$ is the Reynolds number, and $Pr$ is the Prandtl number

$$Re_L = \frac{u_\infty L}{\nu} \qquad \text{and} \qquad Pr = \frac{\nu}{\chi}$$

where $u_\infty$ is the air flow speed, $\nu$ is the kinematic viscosity, and $\chi$ is thermal conductivity of air. In the studied case, the following conditions were used

$$T_\infty = 348\,\text{K}, \qquad T_s = 553\,\text{K}, \qquad u_\infty = 20\,\text{m/s}$$

With the average temperature of 450 K

$$\nu = 32.39 \times 10^{-6}\,\text{m}^2/\text{s}, \qquad \chi = 47.22 \times 10^{-6}\,\text{m}^2/\text{s},$$
$$k = 37.3 \times 10^{-3}\,\text{W/mK}$$

Thus

$$Re_L = \frac{u_\infty L}{\nu} = \frac{20 \times 0.04}{32.39 \times 10^{-6}} = 24\,700$$

$$Pr = \frac{\nu}{\chi} = \frac{32.39 \times 10^{-6}}{47.22 \times 10^{-6}} = 0.686$$

$$\begin{aligned}\overline{Nu_L} &= 0.664 Re_L^{1/2} Pr^{1/3} \\ &= 0.664 \times (24\,700)^{1/2} (0.686)^{1/3} \\ &= 92.04\end{aligned}$$

and

$$\overline{h} = \frac{\overline{Nu_L} k}{L} = \frac{92.04 \times 37.3 \times 10^{-3}}{0.04} = 86\,\text{W/m}^2\,\text{K}$$